Mechanical properties and fracture behavior of an Al–Mg–Sc–Zr alloy at ambient and subzero temperatures

D. Zhemchuzhnikova*, A. Mogucheva, R. Kaibyshev

Belgorod State University, Pobeda 85,

A B S T R A C T

The tensile properties and fracture behavior of an Al–6%Mg–0.2%Sc–0.08%Zr (by wt%) alloy was examined at temperatures ranging from 77 to 293 K under as-cast conditions and after extensive hot rolling. It was found that in the temperature range 223–293 K this alloy exhibits the Portevin-Le Chatelier (PLC) effect, corresponding to a positive temperature dependence of the yield stress (YS). At $T < 223$ K, the YS and ultimate tensile strength (UTS) tend to gradually increase with decreasing temperature. In the rolled alloy, the ductility increases with decreasing temperature over the entire temperature interval, while the as-cast alloy exhibits a ductile to -brittle transition (DBT) at ~182 K. The hot rolled material exhibits ductile fracture over the entire temperature interval while the as-cast material shows a brittle intergranular fracture at 77 K and a dimple-type ductile mode of transgranular fracture at 293 K. It was found that hot rolling highly enhanced the mechanical properties of this material at cryogenic temperatures and the hot rolled alloy can be considered an advanced material for liquefied natural gas (LNG) structures. The foundations of the mechanical behavior of the Al–Mg–Sc–Zr alloy at cryogenic temperatures are discussed.

1. Introduction

Currently, there exists a great demand for liquefied natural gas (LNG) tanks and superstructures for storage on maritime carriers and offshore drilling rigs [1,2]. Natural gas is stored and shipped in the form of LNG at a cryogenic temperature of ~111 K. To guarantee safety, the structural materials for the cryogenic tanks must exhibit sufficient ductility and toughness at subzero temperatures. Excellent cryogenic ductility and toughness are very important because a floating LNG storage facility and LNG carriers have to be highly reliable and structurally sound with the large load of the tank [1]. In addition, these materials have to be strong enough to account for the reasonable weight of the cryogenic structure [1]. Aluminum alloys of the 5xxx series are appropriate structural materials for subzero temperature applications because their ductility and toughness as well as their strength are higher at subzero temperatures than at room temperature [1,3]. In addition, these alloys exhibit excellent corrosion resistance in saltwater, sufficient weldability and low density. As a result, cryogenic tanks for LNG ships and floating storage facilities are currently fabricated from AA5083 alloy or its latest version (AA5182), which contains ~4.5% Mg. These alloys are used both as wrought material in the form of hot rolled plates with thicknesses ranging from 25 to 50 mm, and as large-scale castings in offshore and ship LNG structures [1–3]. However, these alloys exhibit moderate strength and, therefore, the development of a high strength alloy belonging to 5xxx series is of crucial importance for realizing low weight cryogenic structures.

Two alloying concepts exist for enhancing the strength of Al–Mg alloys [4]. First, the concentration of Mg, the primary alloying element, can be increased from 4.5 to 6% wt. Al–Mg alloys with 6% wt. Mg usually exhibit the highest strength among the alloys of the Al–Mg system [4], but tend to suffer from a lower ductility at cryogenic temperatures relative to aluminum alloys with 4.5% wt. Mg. Second, minor alloying additions of such elements as Sc and Zr may provide upwards of +50% increases in the YS and the UTS in an Al–4.5% Mg alloy [4]. Using the minor alloying approach, an Al–4.5%Mg–0.2%Sc–0.09Zr alloy was recently developed and became commercially available as AA5024 alloy for hydrogen tanks operating at 34 K [4]. Such very low service temperatures, however, are not necessary for LNG structures. Hence, it is feasible to enhance the strength of the AA5024 alloy by increasing the Mg content to 6%. It is worth noting that this approach is not useful for materials used in liquefied hydrogen applications because the ductility and cryogenic toughness of this alloy tend to drop for temperatures lower than 113 K. However, this alloy may be a good candidate for LNG structures, which are used at significantly higher temperatures.

The aim of this research is to demonstrate that this Al–Mg–Sc–Zr alloy exhibits a high proof strength while maintaining similar levels of damage tolerance up to the temperature of liquid nitrogen (77 K). The mechanical properties and fracture behavior of this alloy, denoted here as 1575C Al, were examined at ambient and subzero temperatures under as-cast conditions and after extensive hot rolling.

2. Experimental procedures

The 1575C Al, with a chemical composition of Al–6%Mg–0.35%Mn–0.2%Sc–0.08%Zr–0.07%Cr (in wt%), was manufactured by semi-continuous casting using a water-cooled copper chilled mold with a rectangular shape of dimensions $160 \times 40\ mm^2$, which provided a solidification rate of ~75 K/s. The ingot alloy was then homogenized at 360 °C for 12 h and cut into plates with dimension of $80 \times 80 \times 40\ mm^3$. Half of these plates were rolled at an initial temperature of 633 K with a total reduction of 75% to a final thickness of 10 mm. A two-high mill with internal rollers 300 mm in diameter and 350 mm in length was used.

Tensile specimens were machined from the ingot and sheet to a 35 mm gauge length and 7 mm gauge width; the gauge lengths were parallel to the ingot center line and rolling direction (RD), respectively. Tensile tests were carried out over the temperature interval 77–293 K and with strain rates ranging from 1.4×10^{-5} to $8 \times 10^{-1}\ s^{-1}$ using an Instron 5882 testing apparatus equipped with an Instron 3119-408 cryogenic chamber. The coefficient of instantaneous strain rate sensitivity, $m = d(\ln\sigma)/d(\ln)$, was determined by a series of strain-rate-jump tests [5,6] from 223 to 363 K. The variations in the strain hardening coefficient, $n = d(\ln\sigma)/d(\ln\varepsilon)$, with strain were determined from the σ–ε curves [5,6]. Charpy impact tests were carried out in the temperature range 77–293 K on standard $10 \times 10 \times 55\ mm^3$ specimens with a 2 mm U-notch in accordance with ASTM standard E23-05 using an Instron IMP460 machine with a capacity of 300 J. The longitudinal sections of the specimens were parallel to the central axis of the ingot or RD. The impact values were averaged over three tests at each experimental point.

Samples for optical microscopy, electron back scattering diffraction (EBSD) and transmission electron microscopy (TEM) analyses were cut from the central areas of the ingots and plates along the central line of the ingot and parallel to the RD, respectively. The details of this sample preparation for structural characterization have been reported in a previous work [7]. The black and white lines on the EBSD maps indicate the high-angle boundaries (HABs) and low-angle boundaries (LABs) with misorientations of $2 \le \theta \le 15°$ and $15° \ge \theta$, respectively. The dislocation densities were evaluated using a JEM-2100 transmission electron microscope (TEM) by a method described in previous work [8]. An analysis of the constituent phases was performed with an FEI TECNAI-G2 TEM by a method described here [9]. X-ray diffraction (XRD) was performed with a diffractometer using CuKα radiation. Internal elastic strain and coherent domain size were estimated by the Williamson–Hall method [10] using a Rigaku Ultima IV diffractometer.

3. Results

3.1. Initial structures

3.1.1. Structure after solidification followed by homogenization annealing

Fig. 1a shows a typical cell-type uniform structure [9] with an average cell size of ~22 μm. The fraction of HABs and the average misorientation are 87% and 38°, respectively (Fig. 1b). The density of lattice dislocations is relatively low ($\rho \sim 3 \times 10^{12}\ m^{-2}$), and no internal elastic strain was detected by X-ray analysis.

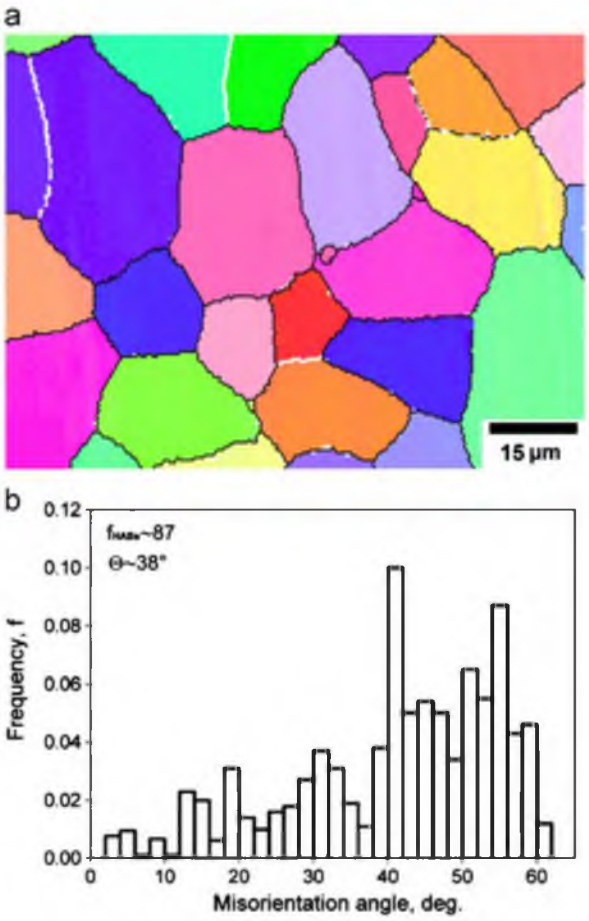

Fig. 1. Microstructure of the as-cast 1575C Al.

The EDX analysis revealed the presence of two main phases: Al_3Sc and Al_6Mn (Fig. 2). Two types of Al_3Sc dispersoids were found. The coherent Al_3Sc dispersoids had an average size of ~10 nm and were very uniformly distributed within the matrix, while the incoherent Al_3Sc particles with an average size of ~40 nm precipitated on boundaries (Fig. 2). The average content of Sc in the Al_3Sc phase is ~6% wt. The incoherent dispersoids were identified as an Al_6Mn phase with an average diameter of ~25 nm and plate-like or round shapes and were primarily observed within the grain interiors. No evidence for the precipitation of any β-phase (Al_3Mg_2) or Al_3Cr phase was found. The elemental mapping of Mg, Mn, Sc, Zr, Cr, and Fe elements shows that Mg, Zr and Cr are uniformly distributed within the Al matrix (Fig. 3), and therefore, form a substitutional solid solution. In contrast, the Mn and Sc are non-uniformly distributed within the Al matrix (Fig. 3); the majority of these elements were consumed for the formation of the Al_3Sc and Al_6Mn dispersoids.

3.1.2. Microstructure after hot rolling

Hot rolling led to the formation of a deformation microstructure consisting of lamellar grains aligned along the RD that contains deformation bands and an increased density of lattice dislocations (Fig. 4). The average grain thickness and longitudinal length are ~6 and ~52 μm, respectively (Fig. 4). Deformation bands delimited by extended LABs are aligned with the RD or oriented at ±40° to the RD within the interiors of the lamellar

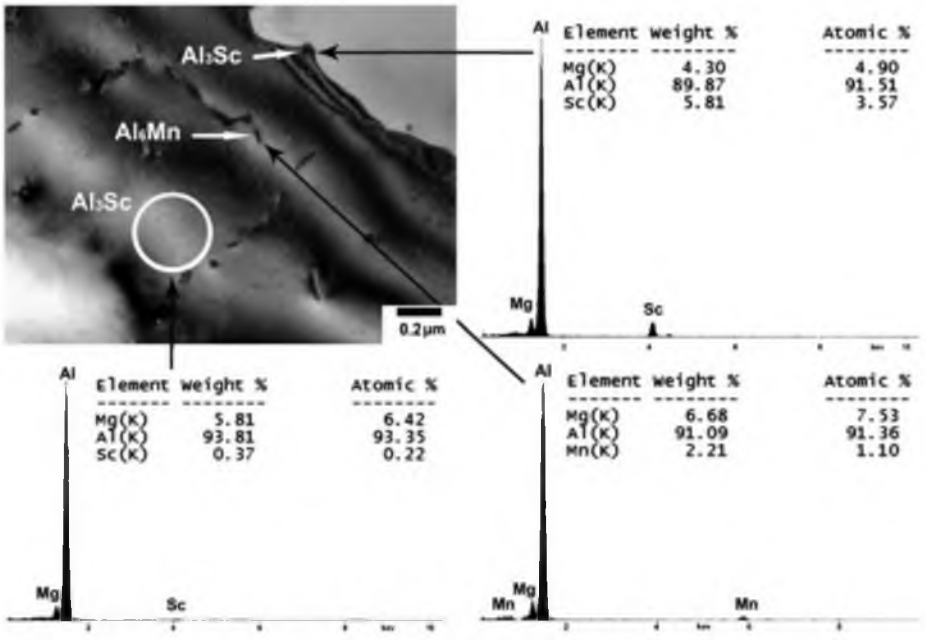

Fig. 2. TEM image of the as-cast 1575C Al and EDX analysis of the particles.

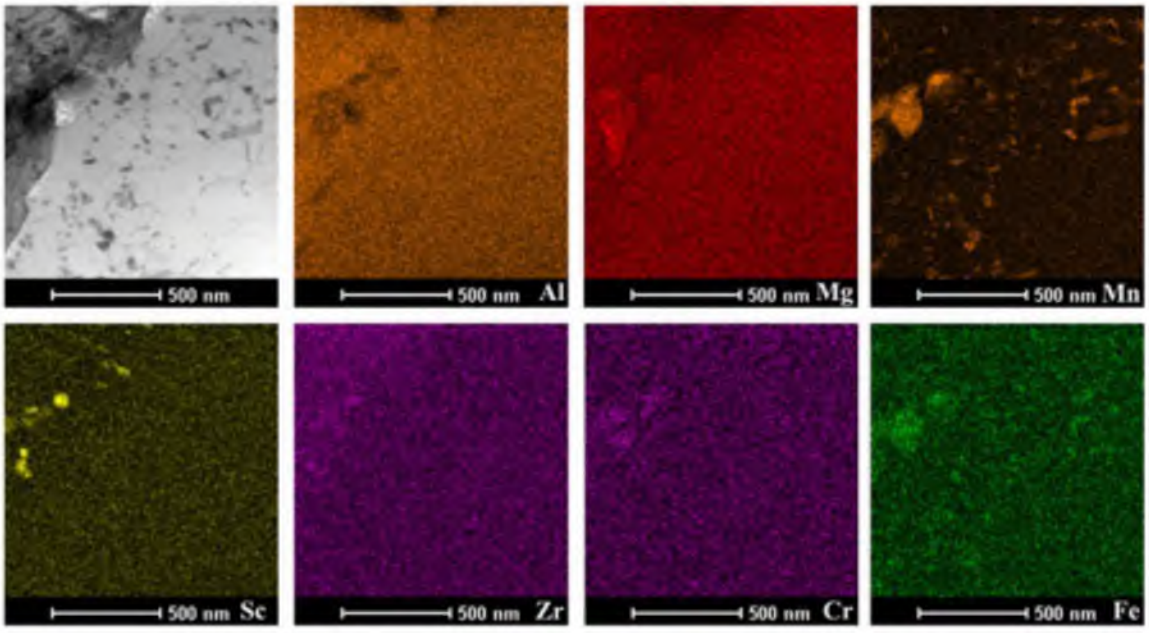

Fig. 3. Distribution of elements in the selected plane of the as-cast 1575C Al.

grains (Fig. 4a and b). The TEM study revealed the existence of a regular array of parallel deformation bands subdivided by transverse boundaries that have a very low misorientation (Fig. 4b) on the subgrains with an average thickness and length of ~0.3 and ~0.7 μm, respectively (Fig. 4a). A moderate dislocation density ($\rho \sim 4 \times 10^{13}$ m^{-2}) was found within them. There exists a strong attractive interaction between the Al_6Mn particles and the Al_3Sc phases and lattice dislocations (Fig. 4c). Chains of secondary phase particles located within the interiors of the grains were also found. It is apparent that the dynamic detachment of the initial boundaries from chains of relatively coarse particles took place during rolling. The fraction of LABs is ~83%; the average misorientation is ~10° (Fig. 4d) and the internal elastic strain attained is ~0.14%. Thus, hot rolling resulted in the formation of a well-defined subgrain structure; and the density of lattice dislocations increased by a factor of ~11. It is worth noting that this deformation structure can be distinguished from a typical cold rolled aluminum structure [11–14] by the presence of only one set of deformation bands within each initial grain and a lower dislocation density, which is lower by a factor of ~5.

3.2. Mechanical properties

3.2.1. Tensile properties

The engineering stress–strain curves of the 1575C Al at a strain rate of 10^{-3} s^{-1} and the yield stress (YS) ($\sigma_{0.2}$), ultimate tensile strength (UTS) (σ_B) and total elongation-to-failure (δ) are presented in Fig. 5 and Table 1.

In the as-cast alloy the flow stress tends to increase with decreasing temperature, while the ductility tends to increase until

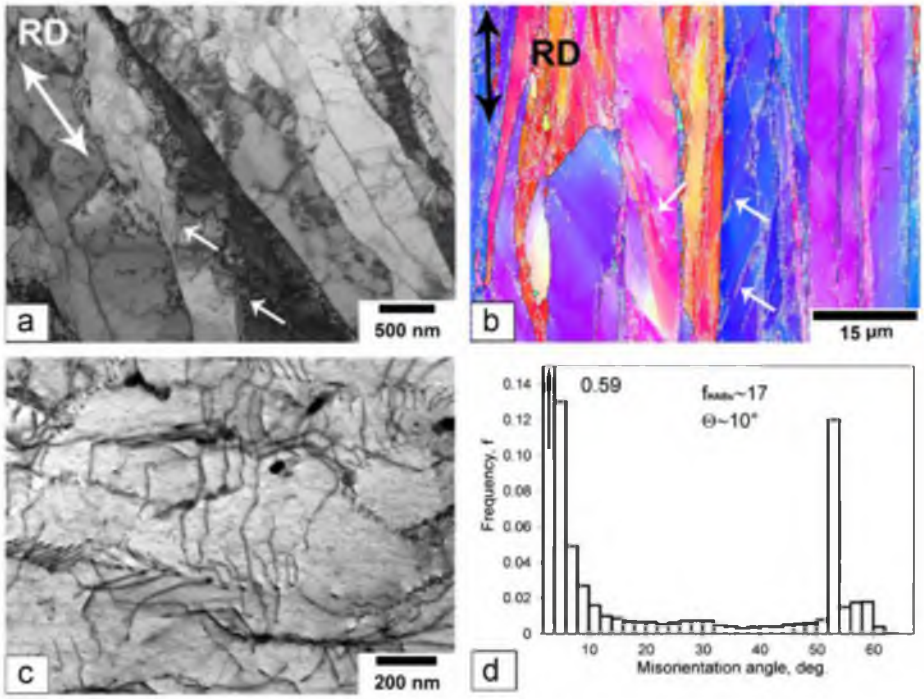

Fig. 4. Microstructure of the 1575C Al after rolling. Arrows indicate the deformation bands.

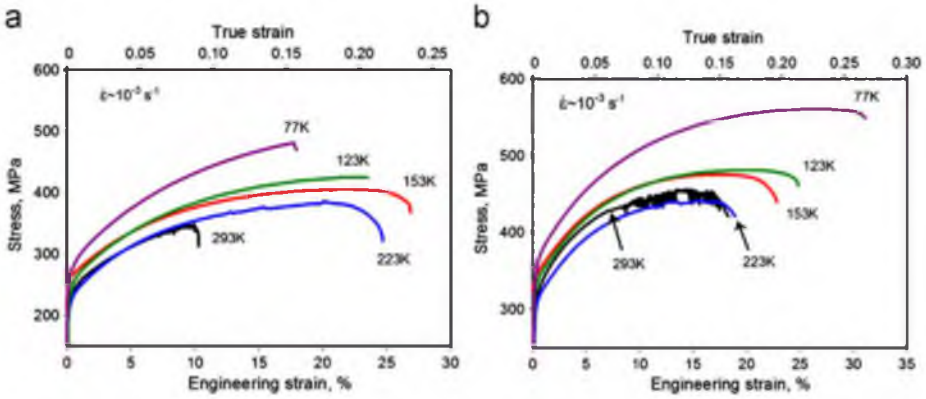

Fig. 5. Effect of temperature on the stress–strain curves for the 1575C Al in (a) as-cast state and (b) after rolling.

Table 1
Tensile properties of aluminum alloy 1575C.

Temperature (K)	Mechanical properties					
	As-cast state			After rolling		
	$\sigma_{0.2}$ (Mpa)	σ_s (MPa)	δ (%)	$\sigma_{0.2}$ (MPa)	σ_s (MPa)	δ (%)
293	225	360	12	295	450	20
223	208	383	24	288	440	19
153	220	400	25	300	475	22
123	240	430	23	315	485	25
77	260	470	16	335	555	34

attaining a maximum at 153 K (Fig. 5a). At $T < 153$ K, the ductility decreases with decreasing temperature. These non-monotonous temperature dependencies of strength and ductility are attributed to three types of σ–ε curves that can be distinguished at different temperatures (Figs. 5a and 6a). At room temperature, the serrated flow is manifested as repeating oscillations on the stress–strain curves (Fig. 5a). This phenomenon is generally associated with the Portevin Le Chatelier (PLC) effect attributed to dynamic strain aging (DSA) [15–18]. Two types of serrations are observed. The so-called type A serrations are distinguished as an abrupt rise in the stress followed by a drop to or below the general level of flow stress on the σ–ε curve that is manifested at ambient temperature. This type of serration arises from the repetitive continuous propagation of deformation bands from one end of the gauge to the other [15]. It is known [15–18] that plastic instability attributed to PLC effects yields low ductilities. At room temperature, the strain hardening coefficient, n, highly increases from 0.03 at very small strains of ~0.01 to ~0.5 at $\varepsilon \sim 0.07$ that should provide sufficient ductility. However, the n value drops upon further deformation (Fig. 6a) due to appearance of the PLC effect. In addition, a very low m value (-0.2) (Fig. 6a) yields significant plastic instability [19,20]. As a result, the elongation-to-failure is only slightly higher than the critical strain at which serrations on the stress–strain curve appears [16–18]. It is worth noting that a positive temperature dependence of the flow stress observed in the present work at $T \geq 223$ K as in [21] is a direct manifestation of the negative strain-rate sensitivity, m [19,20] (Fig. 7a).

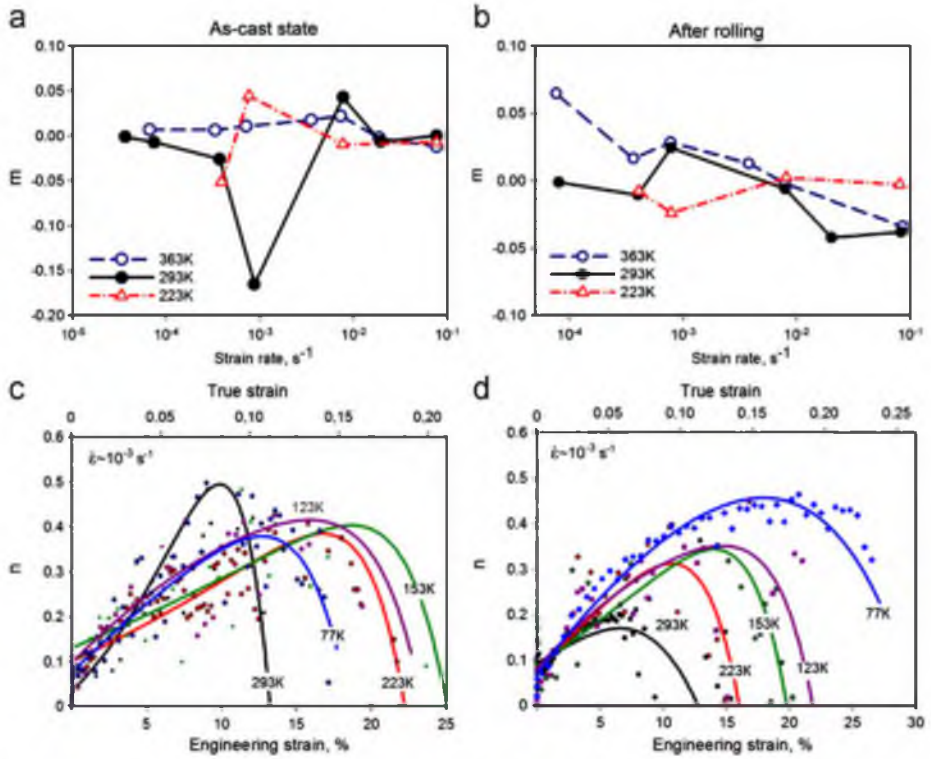

Fig. 6. Strain rate sensitivity parameter and the strain hardening coefficient of 1575C Al in (a, b) as-cast and (a', b') hot rolling conditions.

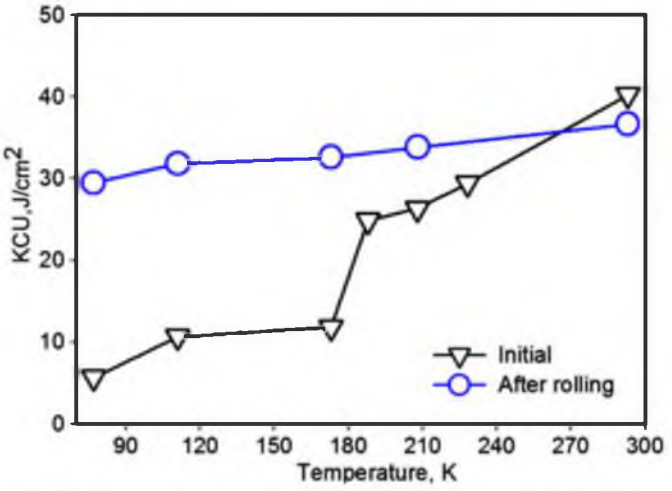

Fig. 7. Temperature dependencies of the impact energy for the 1575C Al.

At T=223 K, the alloy shows evidence of type E serrations (Fig. 5a), which have the same origin as the type A serrations and often appear after them [15]. We can assume that transition from type A to type E serrations can be attributed to a significant increase in the m value with decreasing temperature (Fig. 7a).

In the temperature interval 153–223 K, no evidence of the PLC effect was found and the σ–ε curves exhibit apparent steady state conditions at $\varepsilon \geq 0.15$ (Fig. 5a). The n value gradually increases from ~0.1 at small strain to ~0.38 just before attaining steady state flow and then tends to decrease to zero (Fig. 6a). At $T < 153$ K, an increase in strain hardening with strain is observed until failure (Figs. 5a and 6a); where the highest n value is ~0.4. Therefore, no instability of plastic flow [5] takes place. This type of mechanical behavior should result in the attainment a high ductility. It is apparent that premature fracture limits ductility at these temperatures.

At ambient temperature, rolling results in increases in the YS from 225 to 295 MPa, the UTS from 360 to 450 MPa and the elongation-to-failure from 12% to 20% (Fig. 5 and Table 1). The temperature dependence of strength is also not monotonic for the hot rolled 1575C Al, while the ductility tends to increase with decreasing temperature. At ambient temperature, the hot rolled alloy exhibits type B serrations (Fig. 5b), in which oscillations appear with high frequency stress jumps. This type of jerky flow corresponds to a hopping propagation of localized bands at room temperature [15]. The serrations changing from type A to type B usually takes place with increasing temperature [15]. It can be seen that in the 1575C Al, this transition also occurs due to hot rolling.

At 223 K, the hot rolled alloy shows the lowest strength (Fig. 5b and Table 1), this is attributed to the transition to type E serrations [20–22]. At the same time, at $T \leq 223$ K, the m value (Fig. 6a') is ~0 over a wide strain rate interval, and the n value gradually increases from ~0.1 at small strain to ~0.3 at ε~0.15 (Fig. 6b'). As a result, the ductility is sufficiently high. At $T < 223$ K, an extensive increment in the strain hardening with strain (Fig. 5b) results in an increased stability of plastic flow and high ductility. For instance, at room temperature and $T \leq 153$ K, the highest n values are ~0.18 and $\geq$0.45 (Fig. 6b'), respectively. It seems that no premature fracture takes place at subzero temperatures, and, as a result, the hot rolled alloy is sufficiently ductile even at 77 K (Fig. 5b and Table 1). The YS and UTS gradually increase with decreasing temperature.

3.2.2. *Impact testing*

The effect of temperature on the Charpy U-notch impact energy is shown in Fig. 7. The as-cast alloy exhibits a well-defined ductile-brittle transition (DBT) in the temperature interval 180–200 K.

The impact toughness drops from 24 to 12 J/cm^2 and for $T < 180$ K, the value of the Charpy U-notch impact gradually decreases to 6 J/cm^2 with decreasing temperature (Fig. 7). However, this value is essentially equal to the Charpy impact energy at room temperature of high-performance grades of traditional Al–7%Si casting [23]. In contrast with the as-cast alloy, the impact toughness of the hot rolled 1575C Al gradually decreases with decreasing temperature (Fig. 7). However, even at 77 K, the value of the Charpy U-notch impact is 28 J/cm^2, which is high enough for use as a structural material. No DBT is observed at $\geq$77 K. Therefore, the hot rolled 1575C Al is not susceptible to embrittlement at cryogenic temperatures $\geq$77 K.

3.3. *Microstructure and fractography after tension*

TEM observations revealed that the main difference in microstructural evolution during tension between the two states of the 1575C Al alloy consisted of deformation banding; the hot rolling highly promotes the formation of thin deformation bands under tension. In the as-cast material at ambient temperature, a rare formation of planar LABs expanding from one initial boundary to another takes place. These deformation bands have thicknesses ranging from 0.2 to 1 μm and are visible within a very limited number of initial grains (Fig. 8a and b). The fraction of the LABs increases to 31% and the average misorientation decreases to 25° (Fig. 8c, Table 2). However, misorientation of the LABs is low on average. As a result, LABs are rarely detected by EBSD analysis. The dislocation density increased by a factor of ~15 up to $\rho \sim 5 \times 10^{13}$ m^{-2} and the internal elastic strain rises to 0.3% (Table 2). It is worth noting that chains of relatively coarse particles of Al_6Mn and $Al_3(Sc,Zr)$ secondary phases are observed along the initial grain boundaries (Fig. 8a). A temperature decrease to 77 K leads to an increase in the lattice dislocation density up to $\rho \sim 2 \times 10^{14}$ m^{-2} and suppresses the formation of coarse deformation bands (Fig. 8a′–c′, Table 2).

In the hot rolled 1575C Al the initial grains are subdivided by deformation-induced LABs into numerous deformation bands by the

Table 2
The measured values of the average misorientation angle (θ), the fraction of high angle boundaries (fHABs) the density of lattice dislocations (ρ) and the internal elastic strain for the 1575C Al after tensile testing.

Condition	Temperature (K)	θ (deg.)	fHABs (%)	ρ (m^{-2})	Local strain (%)
As-cast	293	25	69	5×10^{13}	0.302
	77	29	70	2×10^{14}	0.218
After hot rolling	293	18	36	3×10^{14}	0.402
	77	15	29	5.6×10^{14}	0.360

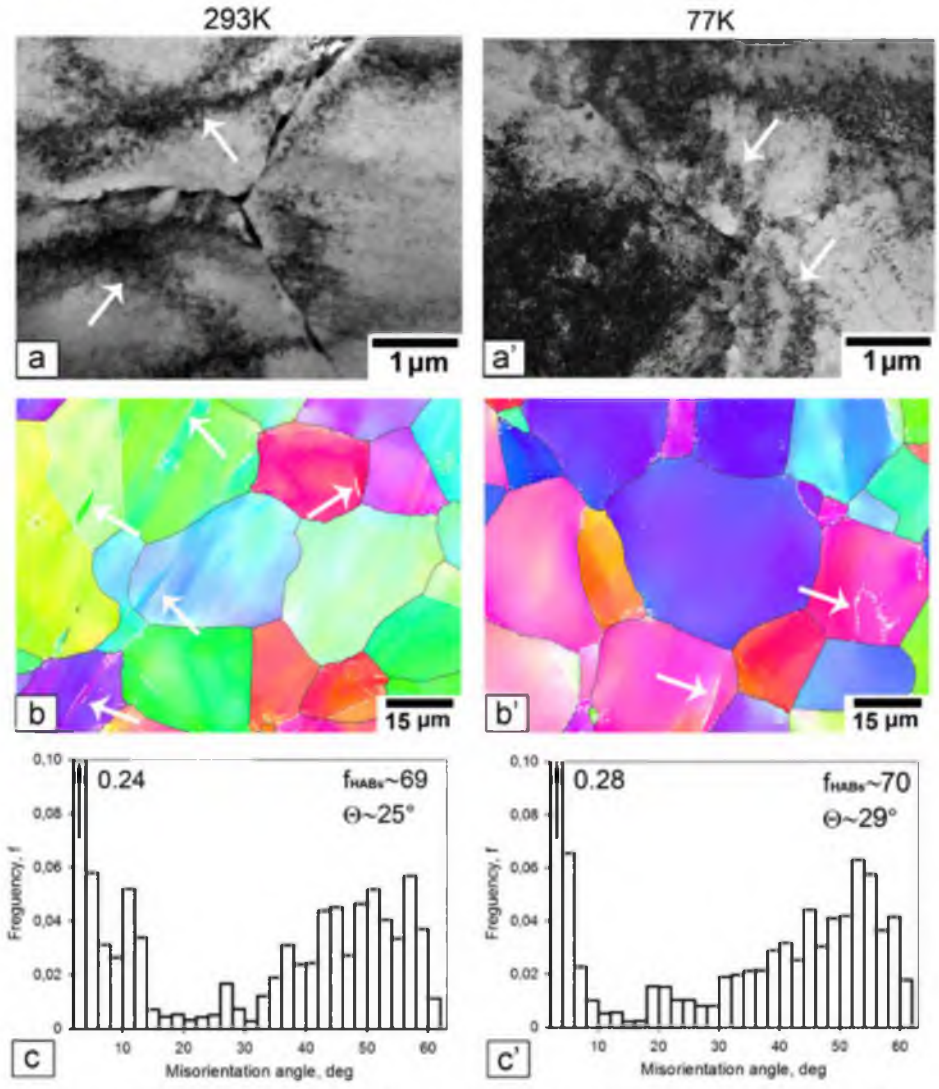

Fig. 8. Microstructure of the as-cast 1575C Al after tensile testing at (a–c) 293 K and (a′–c′) 77 K. Arrows indicate the deformation bands.

LABs (Fig. 9a). The initial grains are highly elongated (Fig. 9b). As a result, the coarse deformation bands have a low average longitudinal dimension, which is close in thickness to the initial grains (Fig. 9b). At ambient temperature, the average misorientation increases to 18° and the proportion of LABs decreases to 64%, the dislocation density increases by a factor of ~8 to $\rho \sim 3 \times 10^{14}\ m^{-2}$, leadings to a high internal stress (Fig. 9c, Table 2). At 77 K, the density of deformation bands is higher than at 293 K, and their thickness is decreased. As a result, a portion of the LABs and their average misorientation are 71% and 15°, respectively (Fig. 9a′–c′, Table 2). A high dislocation density of $\sim 5.6 \times 10^{14}\ m^{-2}$ evolves (Fig. 9a′, Table 2). However, this density induces a slightly lower long-range elastic strain compared to the strain at room temperature (Table 2). It seems that the subdivision of the initial grains into crystallites by the LABs provides a decreased value of the internal elastic strain (Table 2). Thus, in the hot rolled 1575C Al, decreasing the temperature from 293 to 77 K leads to an increase in the lattice dislocation density by a factor of ~2 and a decrease in the internal long-range elastic stress. No formation of coarse deformation bands was detected at cryogenic temperatures. It is worth noting that no chains of secondary phase particles along the boundaries were observed (Fig. 9a and a′).

SEM fractographs of the tensioned specimens are shown in Fig. 10. At room temperature, the as-cast material shows dimple rupture associated with considerable plastic deformation [24] as the main fracture mechanism (Fig. 10a). The second phase particles that are typically present at the bottom of most conical dimples that have essentially equiaxed shapes are indicative of fracture initiated by the separation of secondary phase particles from the aluminum matrix. There exist single nucleation sites for the majority of the microvoids that can grow to large sizes before coalescing (Fig. 10a). Failure primarily occurs along a transgranular fracture path [24].

The fracture mode in the as-cast alloy changes greatly from ductile transgranular to intergranular brittle with decreasing temperature. At 153 K, cracks propagated along the initial boundaries, resulting in the formation of a typical faceted "rock candy" [24] fracture surface (Fig. 10b). However, the material undergoes considerable plastic deformation under the propagation of intergranular cracks; a high density of slip features is observed at the fracture surface of some grains (Fig. 10b). At 77 K, intergranular brittle fracture by cleavage becomes the dominant mode of the rupture process (Fig. 10c).

At room temperature, in the hot rolled 1575C Al, ductile transgranular fracture occurs (Fig. 10a′). Very fine dimples are observed on the fracture surface (Fig. 10a′). It is obvious that numerous nucleating sites are activated. Adjacent microvoids can coalesce before they have an opportunity to grow to a larger size

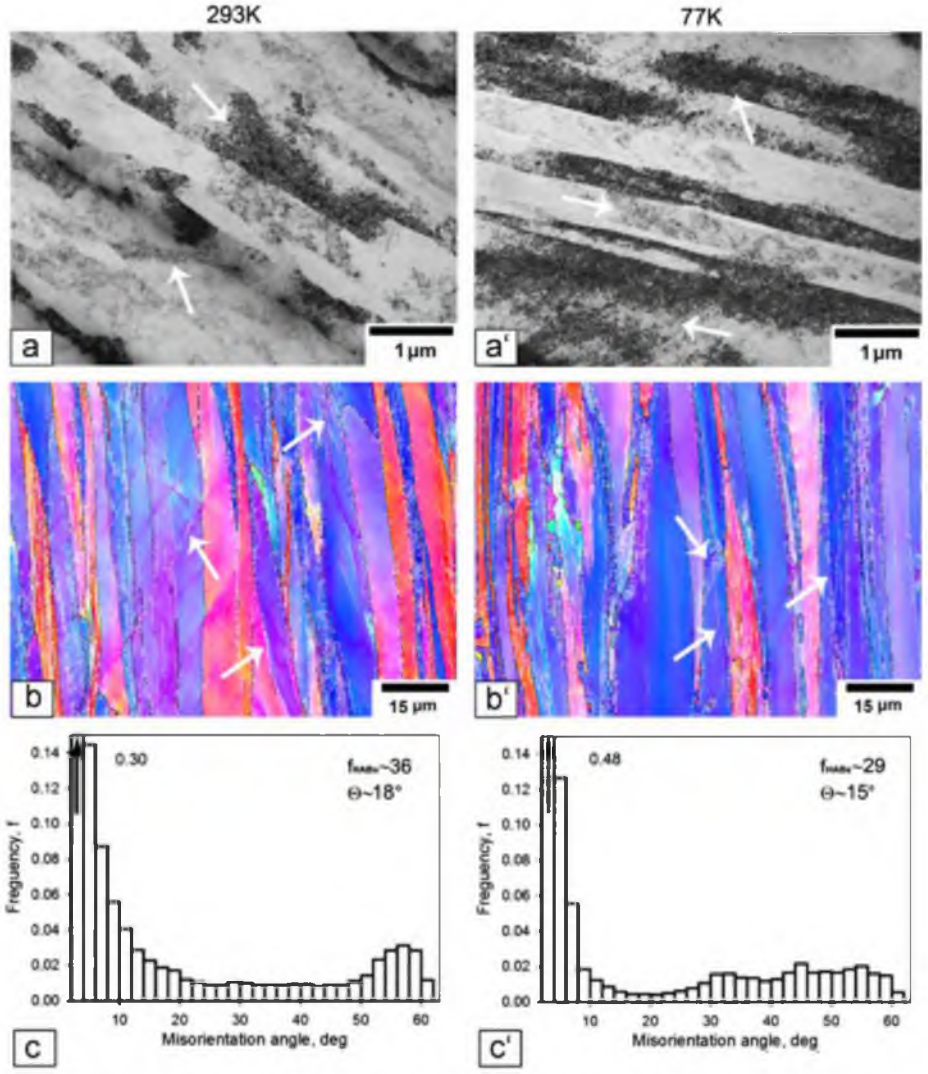

Fig. 9. Microstructure of the rolled 1575C Al after tensile testing at (a–c) 293 K and (a′–c′) 77 K. Arrows indicate the deformation bands.

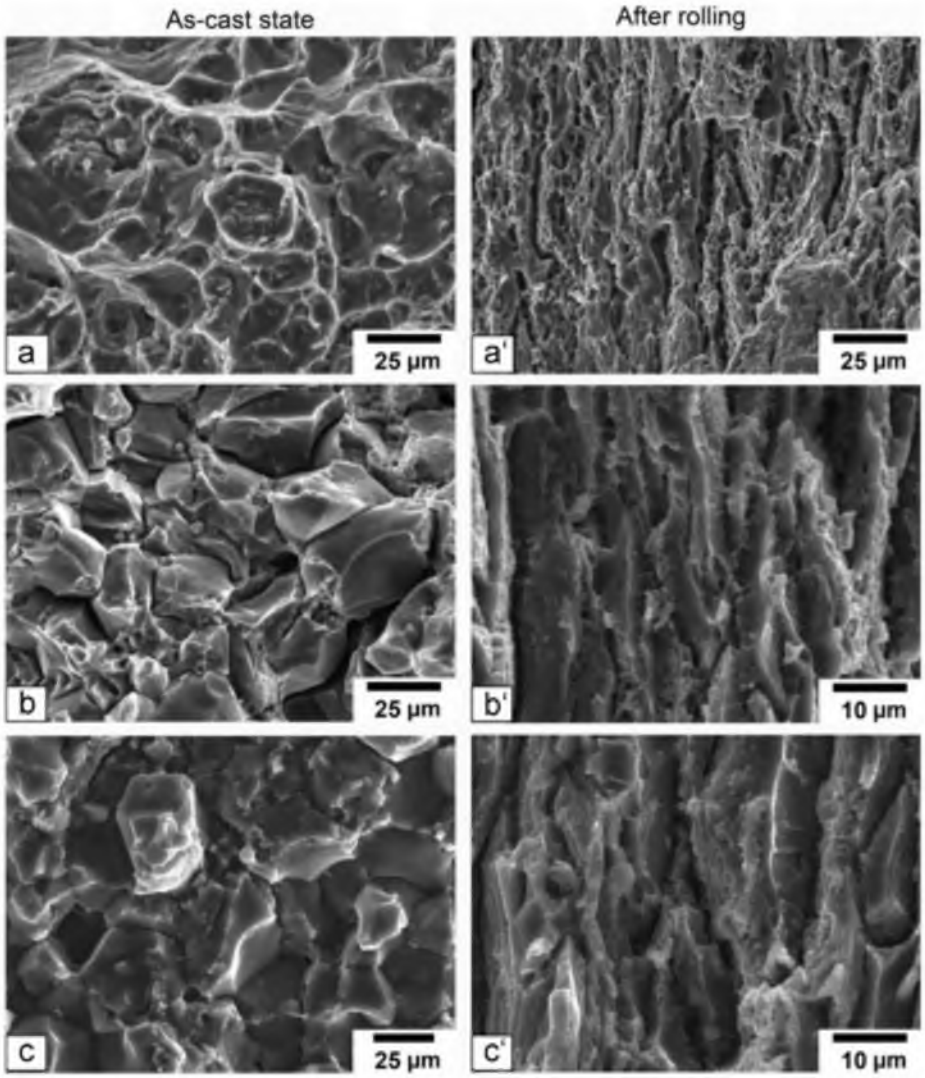

Fig. 10. SEM of the tensile fracture surface of the 1575C Al specimens in the as-cast state and after rolling deformed at temperatures: (a, a') 293 K, (b', b') 153 K, (c, c') 77 K.

only in separate areas near the initial boundaries (Fig. 10a'). These dimples have highly elongated shapes. However, their proportions are insignificant. Particles of secondary phases are rarely observed on the bottom of these elongated dimples. The fracture mode does not change significantly with decreasing temperature (Fig. 10b' and c'), while intergranular fracture along the boundaries of elongated grains could be occasionally observed. Transgranular fracture is high even at 77 K. However, decreasing temperature facilitates the coalescence of microvoids but this does not lead to premature fracture.

3.4. Fractographic observation after the impact test

Above the DBT temperature, fracture primarily occurs in a ductile transgranular manner in the as-cast 1575C Al (Fig. 11a). Intergranular fracture leads to rupture below the DBT temperature (Fig. 11b). However, crack propagation along the boundaries induces considerable plastic deformation despite the fact that cleavage of the grain interiors takes place (Fig. 11b). Decreasing the temperature lowers this plastic deformation (Fig. 11c). Dimples indicating ductile transgranular fracture were rarely found.

In the hot rolled 1575C Al, ductile transgranular fracture dominates at all temperatures (Fig. 11a'–c'). Specific features of this material include a great number of highly elongated dimples; and, adjacent microvoids coalesce along the boundaries of highly elongated grains. Second phase particles are occasionally observed on the bottom of the dimples. It seems that rupture is initiated by crack propagation along boundaries. However, in contrast with the as-cast material, the role of intergranular dispersoids in the initiation of fracture process is unimportant. Decreasing temperature leads to an increased number of these dimples (Fig. 11b'), and at 77 K, evidence of intergranular fracture along boundaries can be found (Fig. 11c'). However, final decomposition requires extensive plastic deformation within the grain interiors (Fig. 11c'). Transgranular fracture occurs in a mixed ductile–brittle manner; ductile fracture provides the primary contribution to overall failure even at liquid nitrogen temperature.

4. Discussion

Inspection of the experimental results shows that the wrought 1575C Al is suitable for cryogenic applications over a wide temperature range. Increased Mg content and Sc and Zr additions provided upwards of a +100% YS increase relative to the AA5182-O alloy [20]. However, the ductility of the hot rolled 1575C Al and AA5083 in O and H111 conditions [20,21] are essentially the same over the temperature interval 77–293 K. Therefore, additional alloying provided a twofold increase in strength without any

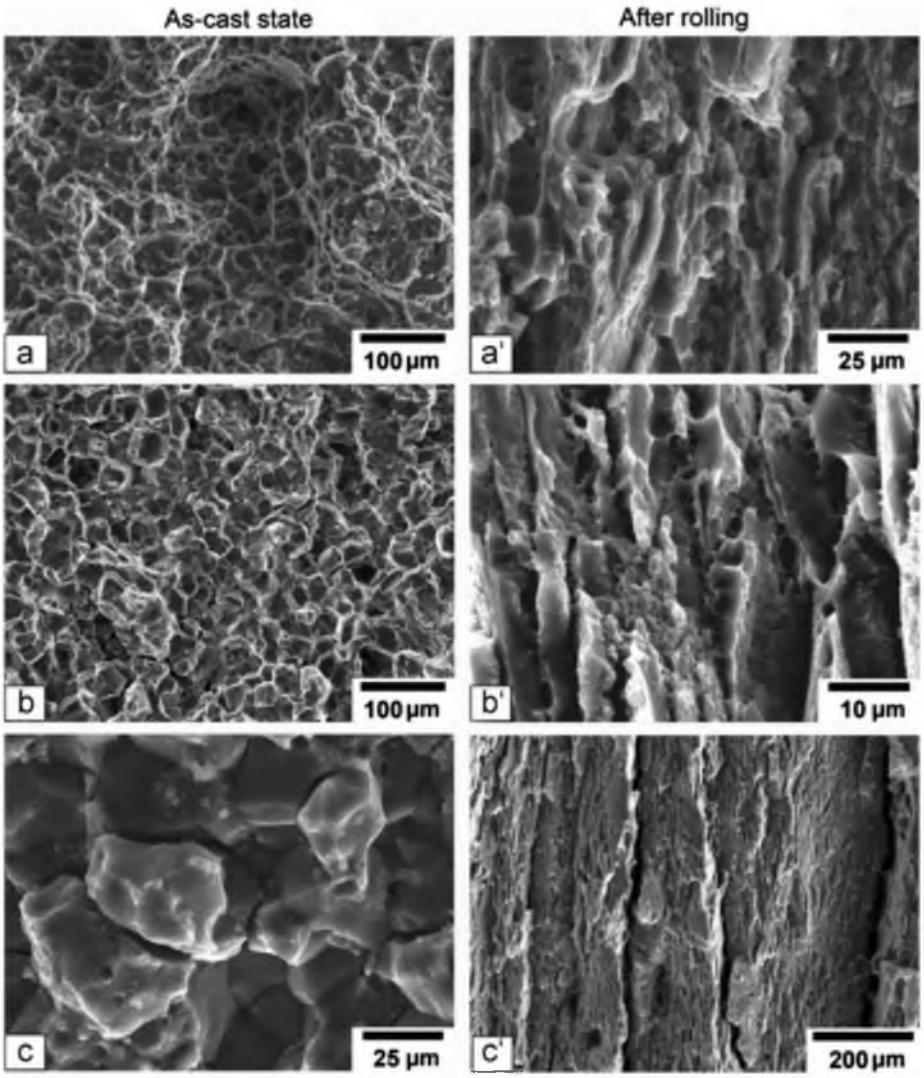

Fig. 11. SEM of specimens of 1575C Al in the as-cast and hot rolled conditions after impact testing at temperatures: (a, a') 293 K, (b, b') 162 K (c, c') 77 K.

degradation in ductility and lightweight cryogenic structures can be fabricated from this material. In addition, the wrought 1575C Al is reliable due to its high impact toughness and excellent ductility at $T \geq 77$ K. It is worth noting that the 1575C Al under hot rolled conditions exhibits only slightly lower ductility than that of low-strength AA5754 alloy containing ~3%Mg [25–27] despite the ~250% difference in YS at 77 K.

In contrast, the 1575C Al in the as-cast condition is not useful as a structural material for exploitation at LNG temperatures in critical components because the DBT occurs above the LNG temperature. Hot rolling highly enhances the ductility and fracture toughness of the 1575C Al by diminishing plastic instability at room temperature and eliminating intergranular brittle fracture at cryogenic temperatures. The positive effects of hot rolling on the mechanical properties are attributed to the detachment of the initial HABs from chains of secondary phase particles and the subdivision of the interiors of the initial grains into separate crystallites. As a result, the first, brittle intergranular fracture along the HABs does not occur, and additionally, the propagation of deformation bands at the macroscale is hindered. In addition, microstructural changes associated with hot rolling provide an increase in strength due to deformation hardening. Hot rolling highly facilitates the formation of thin deformation bands and extensive accumulation of lattice dislocations under tension.

It is known that a high ductility is attained if plastic stability in tension occurs [5]. Numerous works have demonstrated that if $n+m>0.4$ [5,6], no plastic instability takes place over a wide strain interval. There exist two temperature intervals distinguished by the stability of plastic flow. The first temperature range is the PLC domain [15] which the m values are negative or near zero (Fig. 7) due to the formation of coarse deformation bands (Fig. 10b and b') and ductility is limited by plastic instability. Hot rolling suppresses the propagation of coarse deformation bands within the entire grain. This yields a transition from type A with negative values of the stain rate sensitivity coefficient to type B serrations with m values close to zero. It seems that plastic instability is attributed to the formation of coarse deformation bands that highly decreases the m value. As a result, the hot rolled alloy shows significantly higher ductility than the as-cast material despite the lower n values (Fig. 6).

The second domain is over cryogenic temperatures, where the n values in the hot rolled alloy are higher than those in the as-cast material, because accumulation of lattice dislocations under tension is facilitated by decreasing temperature. As a result, the ductility of the hot rolled alloy increases with decreasing temperature. The n values in both states of the 1575C Al are high enough to provide plastic stability. However, the ductility of the as-cast material is restricted by brittle fracture in accordance with

the well-known Yoffee diagram. Chains of intergranular particles provide a lowering of the brittle fracture stress with decreasing temperature. As a result, under tension the applied stress first reaches the brittle fracture stress at the crack tip that initiates intergranular fracture. At the DBT temperature, the effective YS become higher with the brittle fracture stress, and intergranular cracks start to propagate in a brittle mode. The detachment of initial boundaries from chains of particles located along boundaries under hot rolling conditions hinders intergranular fracture, which occurs in an essentially ductile manner even at liquid nitrogen temperature. In contrast, a commercial Al–3%Mg alloy under O conditions exhibits ductile transgranular fracture up to 4.2 K [26]. Therefore, the design philosophy for high-strength cast Al–Mg alloys is primarily in prevention of particle precipitation along grain boundaries. It is apparent that the cast Al–Mg alloy should contain lower amounts of alloying additives relative to the wrought material. In general, the hot rolled 1575C Al exhibits fracture toughness that is half the fracture toughness of the AA5024 alloy at 77 K. However, the present material under hot rolled conditions shows sufficient toughness for applications in LNG structures.

5. Summary

The mechanical properties, fracture behavior and microstructural evolution under tension of Al–6%Mg–0.35%Mn–0.2%Sc–0.08%Zr (in wt%) alloy in the as-cast condition and after isothermal rolling were examined over the temperature interval 77–293 K.

1. The hot rolling of the 1575C Al leads to an elongation of the initial grains, deformation banding, increased dislocation density and detachment of the original boundaries from chains of intergranular particles. At ambient temperature, rolling results in increases in the yield stress from 225 to 295 MPa, the ultimate tensile strength from 360 to 450 MPa and the elongation-to-failure from 12% to 20%.
2. The 1575C Al exhibits the Portevin-Le Chatelier effect in both the as-cast and hot rolled conditions. However, at room temperature, hot rolling changes type A serrations with negative values of the strain rate sensitivity coefficient, m, to type B with an m value close to zero by hindering the formation of coarse deformation bands within initial grains and facilitating the formation of very fine deformation bands. Positive temperature dependencies of the yield stress and ultimate tensile strength in the range 223–293 K are attributed to the PLC effect.
3. The as-cast alloy exhibits a ductile–brittle transition over the temperature interval 180–200 K. The value of the Charpy U-notch impact toughness drops from 24 to 12 J/cm^2 and then gradually decreases to 6 J/cm^2 with decreasing temperature to 77 K due to the facilitation of intergranular brittle fracture at cryogenic temperatures. In contrast, the hot rolled alloy is not susceptible to embrittlement even at 77 K, where the value of the Charpy U-notch impact test is 28 J/cm^2; and a ductile type fracture remains dominant over the entire range of cryogenic temperatures. As a result, at $T < 180$ K, decreasing temperature result in the elongation-to-failure tending to increase in the hot-rolled specimen and decrease under the as-cast conditions.
4. At $T < 223$ K, the yield stress and ultimate tensile strength increase with decreasing temperature in the both conditions. The hot rolled alloy exhibits a higher plastic stability that is associated with strain hardening, which provides an elongation-to-failure of 34% at 77 K, and higher strength, which is attributed to the ease of formation of thin deformation bands and a more extensive accumulation of lattice dislocations under tension relative to the as-cast material.

Acknowledgments

This study was supported by the Federal Agency for Science and Innovations, Russia, under grant No. 16.740.11.0395. The main results were obtained using equipment at the Joint Research Center, Belgorod State University.

References

[1] N. Oiwa, T. Iijima, A. Kida, S. Ohga, J. Light Met. Weld. Constr. 49 (2011) 2–6.
[2] W.S. Park, M.S. Chun, M.S. Hanc, M.H. Kima, J.M. Lee, Mater. Sci. Eng. A 528 (2011) 5790–5803.
[3] J.G. Kaufman, in: M. Kurtz (Ed.), Handbook of Materials Selection, John Wiley & Sons, Inc., New York, 2002, pp. 89–135.
[4] Y.A. Filatov, V.I. Yelagin, V.V. Zakharov, Mater. Sci. Eng. A 280 (2000) 97–101.
[5] J. Pilling, N. Ridley, Superplasticity in Crystalline Solids, The Institute of Metals, London, 1989.
[6] R. Kaibyshev, T. Sakai, I. Nikulin, F. Musin, A. Goloborodko, Mater. Sci. Technol. 19 (2003) 1491–1497.
[7] A. Mogucheva, E. Babich, B. Ovsyannikov, R. Kaibyshev, Mater. Sci. Eng. A 560 (2013) 178–192.
[8] R. Kaibyshev, K. Shipilova, F. Musin, Y. Motohashi, Mater. Sci. Eng. A 396 (2005) 341–351.
[9] M. Gazizov, R. Kaibyshev, J. Alloy Compd 527 (2012) 163–175.
[10] G.K. Williamson, W.H. Hall, Acta Metall. 1 (1953) 22–31.
[11] P.J. Hurley, F.J. Humphreys, Acta Mater. 51 (2003) 1087–1102.
[12] H. Jazaeri, F.J. Humphreys, Acta Mater. 52 (2004) 3239–3250.
[13] G.I. Rosen, D.J. Jensen, D.A. Hughes, N. Hansen, Acta Metall. Mater. 43 (1995) 2563–2579.
[14] Q. Liu, X. Huang, D.J. Lloyd, N. Hansen, Acta Mater. 50 (2002) 3789–3802.
[15] H. Halim, D.S. Wilkinson, M. Niewczas, Acta Mater. 55 (2007) 4151–4160.
[16] H. Ait-Amokhtar, C. Fressengeas, Acta Mater. 58 (2010) 1342–1349.
[17] Y. Brechet, Y. Estrin, Acta Metall. Mater. 43 (1995) 955–963.
[18] J.M. Robinson, M.P. Shaw, Int. Mater. Rev. 39 (1994) 113–121.
[19] R.C. Picu, G. Vincze, F. Ozturk, J.J. Gracio, F. Barlat, A.M. Maniatty, Mater. Sci. Eng. A 390 (2005) 334–343.
[20] R.C. Picu, Acta Mater. 52 (2004) 3447–3458.
[21] F. Ozturk, S. Toros, S. Kilic, Int. J. Mater. Res. 101 (2010) 1172–1179.
[22] J. Balik, P. Lukac, Acta Metall. Mater. 41 (1993) 1447–1454.
[23] T. Kashyap, S. Murali, K.S. Raman, K.S.S. Murthy, Mater. Sci. Technol. 9 (1993) 189–204.
[24] ASM Handbook 12 (1987) 857.
[25] F. Ozturk, S.Toros, H. Pekel, Mater. Sci. Technol. 25 (7) 919–924.
[26] D.-Y. Park, M. Niewczas, Mater. Sci. Eng. A 491 (2008) 88–102.
[27] G. Horvath, N.Q. Chinh, J. Gubicza, J. Lendvai, Mater. Sci. Eng. A 445–446 (2007) 186–192.